A method for measuring the spin polarization of ^{129}Xe by using an atomic magnetometer

Linlin Chen, Binquan Zhou, Guanqun Lei, Wenfeng Wu, Yueyang Zhai, Zhuo Wang, and Jiancheng Fang

Citation: AIP Advances **7**, 085221 (2017);
View online: https://doi.org/10.1063/1.4998732
View Table of Contents: http://aip.scitation.org/toc/adv/7/8
Published by the American Institute of Physics

A method for measuring the spin polarization of ^{129}Xe by using an atomic magnetometer

Linlin Chen, Binquan Zhou,[a] Guanqun Lei, Wenfeng Wu, Yueyang Zhai, Zhuo Wang, and Jiancheng Fang
School of Instrumentation Science and Opto-Electronics Engineering, Beihang University, Beijing 100191, China

(Received 27 May 2017; accepted 2 August 2017; published online 25 August 2017)

We propose a method for the precise determination of nuclear spin polarization, based on the atomic magnetometers, which employs the effective magnetic field produced by the spin polarization of ^{129}Xe nuclei. This effective magnetic field can be estimated by measuring the initial induced voltage of the Free Induction Decay (FID) signal of the ^{129}Xe nuclei, which is based on the calibration coefficient between the transverse magnetic field and the output voltage signal of the atomic magnetometer, by using an off-resonant transverse driven magnetic field. Compared with the method based on measuring the longitudinal relaxation time of the ^{129}Xe nuclei and the spin polarization of alkali-metal atoms, our method can directly measure the nuclear spin polarization, without being affected by inaccuracies in the measurement of the spin polarization of alkali-metal atoms. [http://dx.doi.org/10.1063/1.4998732]

I. INTRODUCTION

The high spin polarization of hyperpolarized noble gases finds applications in a number of fields, including Magnetic Resonance Imaging (MRI),[1–3] neutron spin filters,[4,5] optical atomic magnetometers,[6–8] spin precession gyroscopes,[9,12] and devices aimed at studying fundamental physics.[10,11] In all these applications, the spin polarization of the ^{129}Xe nuclei influences the detection sensitivity and the Signal-to-Noise Ratio (SNR) of the devices. Therefore, an accurate method should be developed to measure the spin polarization of the ^{129}Xe nuclei.

Cohen-Tannoudji *et al.* first used the Rb atomic magnetometer to detect the absolute polarization of ^{3}He.[13] In that work, a 6 cm diameter vapor cell contains the ^{3}He nuclei at a pressure of 3 Torr was placed close to the second vapor cell containing ^{87}Rb that served as a sensor of an optical-pumping magnetometer. The magnetic field produced by the ^{3}He nuclei is 60 nG, which is detected with a sensitivity $\sim 3 \times 10^{-9}\mathrm{G}/\sqrt{Hz}$. Yashchuk *et al.* used the magnetometer based on nonlinear magneto-optical rotation with frequency-modulated light to detect nuclear magnetization of xenon gas.[14] An average magnetic field of ~10 nG produced by Xenon gas at a pressure of 5 bars on the 10 cm diameter vapor cell is detected with SNR ~ 10. Romalis *et al.* used a spin-exchange-relaxation-free potassium magnetometer to detect the equilibrium ^{129}Xe polarization, which determined by measuring the longitudinal relaxation time T_1 of ^{129}Xe itself and the spin polarization of K atoms.[15] However, the precision of this method is limited by the accuracy in measuring the spin polarization of Rb atoms. Z. Ma *et al.* applied a transverse radio frequency (RF) magnetic field to monitor the ^{87}Rb hyperfine electron paramagnetic resonance (EPR) frequency in order to calculate the spin polarization of the ^{129}Xe nuclei.[18,19] However, the working conditions of the EPR method are not suitable for the atomic magnetometer.

In this work, we present a method to determine the nuclear spin polarization by measuring the initial induced voltage of the FID signal of ^{129}Xe nuclei with an atomic magnetometer based on Rb

[a]bqzhou@buaa.edu.cn

atoms. An off-resonant transverse driven magnetic field is applied, and the calibration coefficient between its amplitude and the output signal of the atomic magnetometer is determined. Based on the initial induced voltage of the FID signal and on the calibration coefficient, we can obtain the effective magnetic field produced by the polarized ^{129}Xe nuclei, and then determine the spin polarization accordingly. This method can guarantee more accuracy and rapidity with respect to techniques based on the longitudinal relaxation time of ^{129}Xe nuclei and the spin polarization of Rb atoms, and EPR methods. Moreover, it is not affected by inaccuracies in the measurement of the spin polarization of Rb atoms.

II. PRINCIPLE

The basic elements of the ^{129}Xe spin polarization measurement system are present in Fig.1. A square glass cell is filled with Rb and ^{129}Xe, N_2 as quenching gas, and ^{4}He as buffer gas. A static magnetic field B_0 is applied along the z axis. A circularly polarized beam propagates parallel to the static magnetic field B_0 to optically pump the Rb atoms. The ^{129}Xe nuclei are polarized by spin-exchange collisions with polarized Rb atoms. A transverse driven magnetic field B_1 is then applied along the x axis to stimulate the ^{129}Xe nuclei precession, which is detected by the *in situ* Rb atomic magnetometer.[20,21] The Bloch equation for the alkali atoms can be written as[12,22,23]

$$\frac{dS_+}{dt} = (i[\omega_0 + \gamma_A B_c \cos(\omega_c t)] - \Gamma_A)S_+ - i\gamma_A(B_x + iB_y)S_z, \tag{1}$$

where $S_+ = S_x + iS_y$, ω_0 is the alkali-metal resonance frequency, γ_A is the gyromagnetic ratio of Rb atoms, $B_c cos(\omega_c t)$ is the applied parametric modulation field in the direction of the static magnetic field, Γ_A is a phenomenological parameter describing the relaxation of the alkali spins, B_x and B_y are the magnetic field components along the x and y axes experienced by the Rb atoms.

Assuming the detection of S_x, the output of a lock-in amplifier demodulated with $\sin(\omega_c t)$ is[12]

$$S_x = \frac{\gamma_A S_z}{\Gamma_A} J_1[J_2 - J_0]B_x, \tag{2}$$

where $J_i = J_i(\frac{\gamma_A B_c}{\omega_c})$ $(i=0,1,2)$ is the Bessel function.

The optical rotation angle of linearly polarized D_1 light is given by[12]

$$\theta = n_A \sigma_0 L \frac{W}{2\Delta} S_x, \tag{3}$$

where n_A is the density of alkali atoms, σ_0 is the absorption cross-section at the D1 line of alkali atoms, L is the optical path length, W is the linewidth of the optical transition, Δ is the detuning frequency of the probe beam.

In our experiment, we measure the optical rotation angle after the cell with a balanced amplified photodetector. Therefore, the output signal of the atomic magnetometer is an voltage signal, which can be expressed as

$$V_0 = AI_i n_A \sigma_0 L \frac{W}{2\Delta} \frac{\gamma_A S_z}{\Gamma_A} J_1[J_2 - J_0]B_x, \tag{4}$$

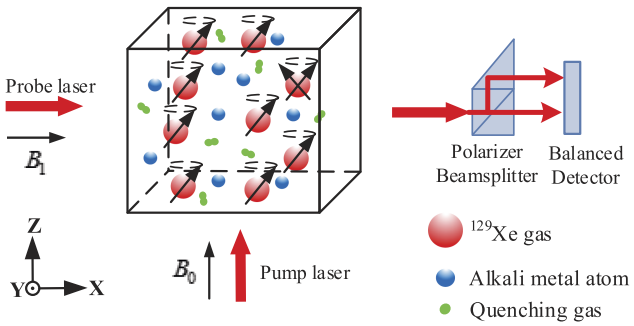

FIG. 1. The basic elements for the measurement of ^{129}Xe spin polarization.

where A is the scale factor between the input differential optical power and the output voltage of the balanced photodetector, and I_i is the probe beam power at the front window of the cell. Since the $AI_i n_A \sigma_0 L \frac{W}{2\Delta} \frac{\gamma_A S_z}{\Gamma_A} J_1 [J_2 - J_0]$ part of Eq. (4) is constant, the output voltage is directly proportional to the magnetic field B_x, which includes the transverse driven magnetic field and the component produced by the polarized ^{129}Xe nuclei.

If an off-resonant transverse driven magnetic field of the form $B_1(t) = B_1 cos(\omega t)$, is applied to the x axis, the polarized ^{129}Xe nuclei are not driven to precess about the z axis. Thus, the transverse magnetic field component of the polarized ^{129}Xe nuclei along the x axis is zero, and the magnetic field B_x equals the off-resonant magnetic field amplitude B_1. The calibration coefficient K between the output voltage of the atomic magnetometer and the magnetic field along the x axis can be thus given by

$$K = \frac{V_0}{B_1}. \tag{5}$$

The off-resonant magnetic field is then turned off, and a $\pi/2$ pulse is applied along the x axis to drive up the ^{129}Xe precession. The output voltage of the atomic magnetometer following the $\pi/2$ pulse corresponds to the FID signal of the ^{129}Xe nuclei. We define V_{FID} as the initial induced voltage of the FID signal, and B_{FID} as the corresponding initial magnetic field, which is proportional to the spin polarization along the z axis of the ^{129}Xe nuclei in thermal equilibrium.[24,25] Therefore, the initial magnetic field B_{FID} based on Eq.(5) can be written as

$$B_{FID} = \frac{V_{FID}}{K}. \tag{6}$$

The effective magnetic field produced by the polarized ^{129}Xe nuclei in thermal equilibrium along the $+z$ axis can be given by[18,26]

$$B_{FID} = \frac{2}{3} k_0 \mu_0 \mu_{^{129}Xe} N_{^{129}Xe} P_{^{129}Xe}. \tag{7}$$

where κ_0 is the Rb-^{129}Xe enhancement factor, μ_0 is the permeability of free space, $\mu_{^{129}Xe}$ is the magnetic moment of the ^{129}Xe nuclei, $N_{^{129}Xe}$ is the number density of ^{129}Xe nuclei, $P_{^{129}Xe}$ is the spin polarization of ^{129}Xe nuclei in thermal equilibrium along the $+z$ axis. The effective magnetic field of the ^{129}Xe nuclei can then be calculated by using Eq. (6), and its nuclear spin polarization can be determined by using Eq.(7), which can be expressed as

$$P_{^{129}Xe} = \frac{3B_1}{2k_0 \mu_0 \mu_{^{129}Xe} N_{^{129}Xe}} \frac{V_{FID}}{V_0}. \tag{8}$$

The voltage signal V_0 and V_{FID} are very sensitive to the variation of the vapor cell temperature, and the power of the pump and probe beam. Thus, based on Eq. (5)(7)(8), the error propagation formulas from the beginning (raw data) to the final result (polarization) can be given by

$$\Delta P_{^{129}Xe} = \pm \frac{3}{2k_0 \mu_0 \mu_{^{129}Xe} N_{^{129}Xe}} \sqrt{\left(\frac{B_1}{V_0}\right)^2 (\Delta V_{FID})^2 + \left(\frac{B_1 V_{FID}}{V_0^2}\right)^2 (\Delta V_0)^2}, \tag{9}$$

$$\Delta K = \pm \frac{\Delta V_0}{B_1}, \tag{10}$$

$$\Delta B_{FID} = \pm \sqrt{\left(\frac{B_1}{V_0}\right)^2 (\Delta V_{FID})^2 + \left(\frac{B_1 V_{FID}}{V_0^2}\right)^2 (\Delta V_0)^2}. \tag{11}$$

III. EXPERIMENTAL SETUP

The experimental setup is shown in Fig. 2. A cubic vapor cell with 4mm and the wall thickness of 1mm, made of quartz glass, is filled with a droplet of Rb atoms, 5 Torr of ^{129}Xe, 20 Torr of N_2 as quenching gas, and 200 Torr of ^{4}He as buffer gas. The vapor cell is placed into an oven and heated

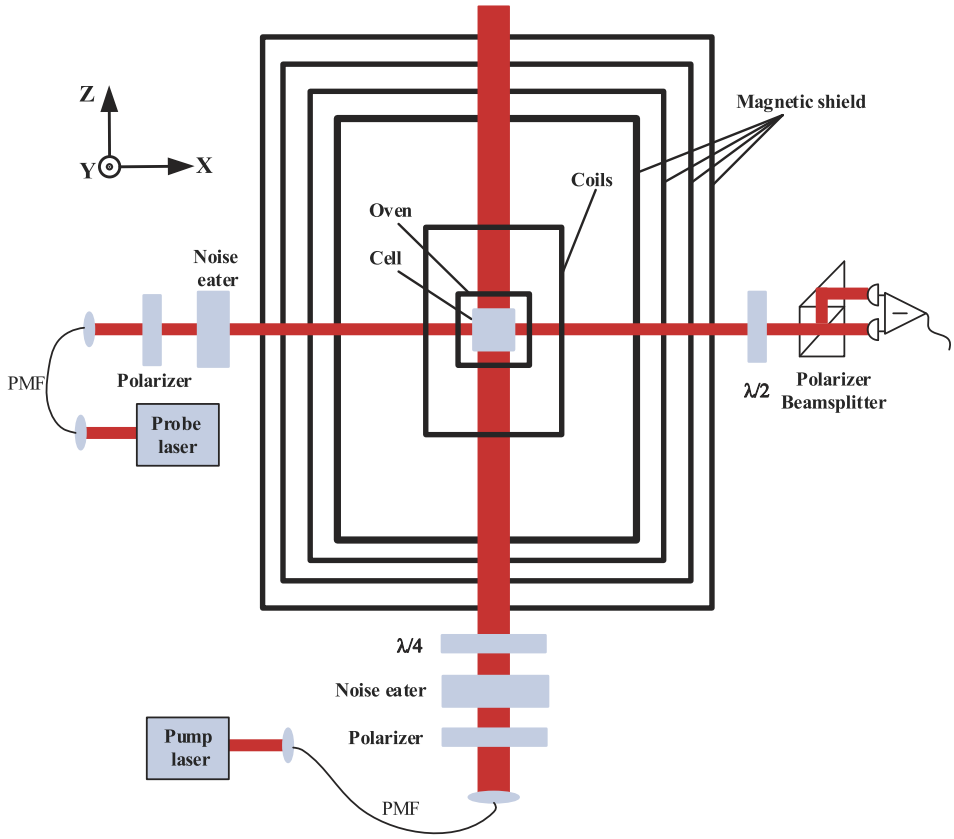

FIG. 2. Experimental setup of the NMRG. The circularly polarized pump beam and the linearly polarized probe beam propagate along the z and x directions, respectively.

to 90-120°C by an electronic heater. A four-layer cylindrical μ-metal magnetic shield is applied in order to reduce the external magnetic field below 10 nT. The residual magnetic field is compensated by three-axis coils inside the magnetic shields.

The circularly polarized pump beam is generated from a Photodigm DBR laser system along the z axis, which is tuned to the D1 line of Rb atoms (794.979 nm). The linearly polarized probe beam, originated from another Photodigm DBR laser system, is detuned by an amount of 50 GHz from the D1 line of Rb atoms in order to detect the magnetometer signal, which is perpendicular to the pump beam at the center of the vapor cell in the x axis. The pump power is set to 1.5 mW, the probe power is low enough (about 0.5 mW) to reduce the effects of the polarization of ^{129}Xe nuclei. The pump and probe powers are stabilized by the Thorlabs Liquid Noise Eater(LCC312H). The output signal of the atomic magnetometer, demodulated by a lock-in amplifier, is acquired using a Model 2307 and a NI PXI-4461 DAQ card with a sample rate of 10KHz.

IV. EXPERIMENTAL RESULTS AND DISCUSSION

In this experiment, the static magnetic field, $B_0 = 10\mu T$, is applied along the z axis. The off-resonant magnetic field, oscillating at a frequency of 104Hz, is applied along the x axis. Fig. 3 shows that the output voltage signal of the atomic magnetometer is directly proportional to the off-resonant magnetic field amplitude B_1 along the x axis. The data were fitted to Eq.(5), yielding a calibration coefficient K=0.134, with an error of 0.00012 based on Eq.(10). The output voltage V_0 was measured at different temperatures, allowing the determination of K at different temperatures as presented in Table I.

The off-resonant magnetic field is then turned off, and the $\pi/2$ pulse is applied along the x axis. The raw signal of the FID at 110 °C is shown in Fig. 4(a). The individual 0.5 s raw data segments is

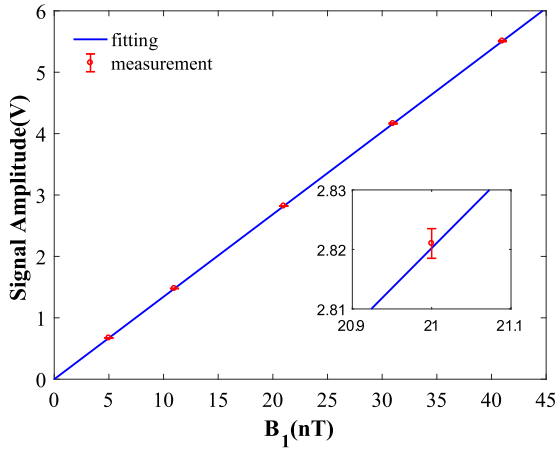

FIG. 3. Output voltage as a function of the off-resonant transverse magnetic field amplitude B_1 along the x axis at 110°C. The amplitude B_1 is set in the range 5-41 nT. The fit based on Eq.(5) gives the calibration coefficient K=0.134±0.00012. The inset shows the magnification of data in the magnetic field interval of 20.9–21.1 nT.

TABLE I. Calibration coefficient of the NMRG at different temperatures.

T(°C)	B_1(nT)	V_0(V)	K(V/nT)
95	21	1.956±0.0014	0.0931±0.000067
100	21	2.121±0.0017	0.101±0.000081
105	21	2.515±0.0021	0.119±0.0001
110	21	2.821±0.0025	0.134±0.00012
115	21	3.191±0.0029	0.152±0.00014

fitted to a function, which is given by

$$V(t) = V_{FID} \exp(-(t - t_0)/T_2) \sin(\omega_L(t - t_0) + \phi), \tag{12}$$

where t_0 is the start time of each raw data segment, T_2 is the transverse relaxation time of ^{129}Xe nuclei, ω_L is the Larmor precession frequency of the ^{129}Xe nuclei, and ϕ is the phase of the ^{129}Xe nuclei. Therefore, we can obtain the FID profile of the raw data as a function of time using Eq.(12), as shown in Fig.4(b). The initial induced voltage value V_{FID} is 0.475 V, with an error of 0.0015 V. The initial magnetic field amplitude B_{FID}=3.545 nT can be calculated from Eq.(6), the error is 0.011 nT based on Eq.(11). Thus, by using Eq.(7), we find that the spin polarization of ^{129}Xe nuclei $P_{^{129}Xe}$ = 1.238%, with an error of 0.0038% using Eq.(9). Fig.4(c) shows that the Larmor precession frequency drift of ^{129}Xe nuclei changes from 128.2751 Hz to 128.2890 Hz in the first 30 s of the FID signal, the maximum and the minimum measurement errors are 0.0018 Hz and 0.0108 Hz, respectively. Fig.4(d) shows that the transverse relaxation time drift of ^{129}Xe nuclei changes from 8.2007 s to 8.2906 s in the first 30 s of the FID signal, the maximum and the minimum measurement errors are 0.0106 s and 0.0762 s, respectively.

Fig. 5(a) shows the initial induced voltage profile of the FID signal at different temperatures. The vapor cell is heated to 95-115 °C. The measured data is fitted to Eq.(12), and the initial induced voltage values V_{FID} at different temperatures are listed in Table II. According to the induced voltage V_{FID} and the calibration coefficient K, we can obtain the initial magnetic field B_{FID}, as well as the spin polarized of ^{129}Xe nuclei $P_{^{129}Xe}$, at different temperatures using Eq. (6) and Eq.(7). The error of the B_{FID} and $P_{^{129}Xe}$ can be calculated by using Eq.(11) and Eq.(9), respectively. The magnetic field and polarization produced by ^{129}Xe are presented in Table II. The spin polarization of the ^{129}Xe nuclei first increases to a maximum at 110°C and then decreases at higher temperatures. This indicates the possibility to optimize the temperature of the vapor cell in order to obtain the highest spin polarization. Fig. 5(b) shows that the Larmor precession frequency drift of ^{129}Xe nuclei at different temperatures. The Larmor precession frequency of ^{129}Xe nuclei first increases

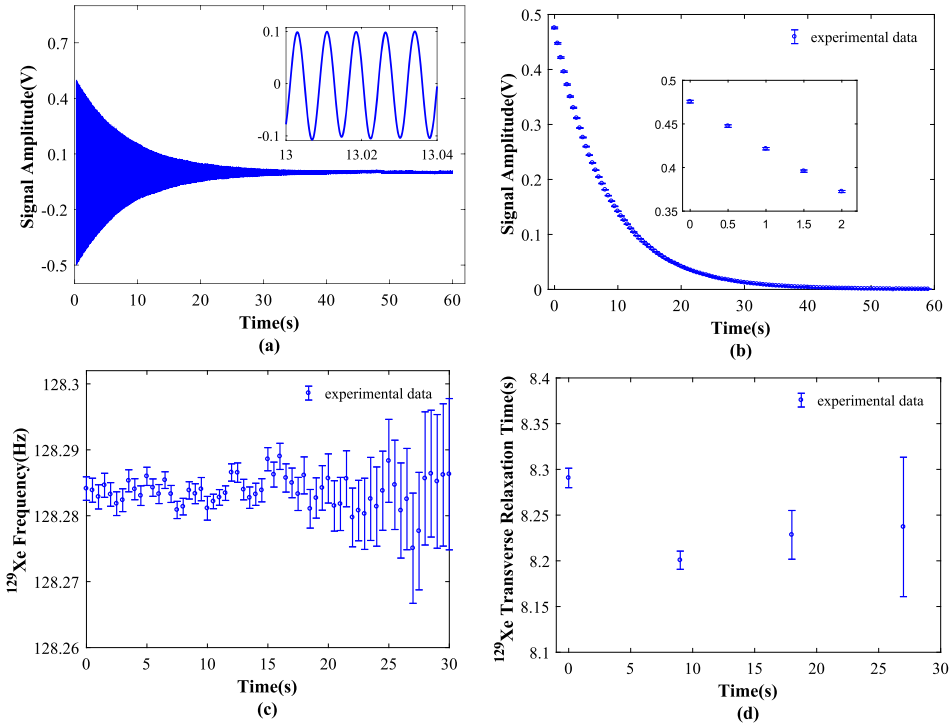

FIG. 4. (a) Raw signal following the $\pi/2$ pulse of ^{129}Xe at a temperature of 110°C. The inset shows the magnification of the data in the time interval of 13–13.04 s. (b) FID profile as a function of time obtained by using Eq.(12), which gives the initial induced voltage V_{FID}=0.475±0.0015 V. The inset shows a close-up of the first 2 s of the signal. (c) The Larmor precession frequency drift of ^{129}Xe nuclei changes from 128.2751 Hz to 128.2890 Hz, the maximum and the minimum measurement errors are 0.0018 Hz and 0.0108 Hz, respectively. (d) The transverse relaxation time drift of ^{129}Xe nuclei changes from 8.2007 s to 8.2906 s, the maximum and the minimum measurement errors are 0.0106 s and 0.0762 s, respectively.

to a maximum at 105°C and then decreases at higher temperatures. Fig. 5(c) shows that transverse relaxation time drift of ^{129}Xe nuclei at different temperatures. We find that the transverse relaxation time of ^{129}Xe nuclei decreases with the temperature. The error bars shown reflect the statistical uncertainty in the all measured quantities based on Eq.(12). Moreover, there are some systematic errors that limit the measurement accuracy of the spin polarization of ^{129}Xe nuclei: these could include, for example, the $\pi/2$ pulse off-resonant frequency effects. In some cases, the initial induced voltage V_{FID} of the FID signal following the $\pi/2$ pulse decreases under the same experimental conditions. These may be because the frequency of the $\pi/2$ pulse is detuned from the Larmor precession frequency of ^{129}Xe nuclei.

The spin polarization of the ^{129}Xe nuclei is affected by the spin polarization of Rb atoms, binary and three-body collisions.[16,17,27] Taking these processes into account, the spin polarization can be calculated with the following equation

$$P_{^{129}Xe} = \frac{R_{se}}{R_{se} + \Gamma_{^{129}Xe}} P_{Rb}, \tag{13}$$

where P_{Rb} is the spin polarization of Rb atoms, R_{se} is the Rb-^{129}Xe spin exchange rate, $\Gamma_{^{129}Xe}$ is the ^{129}Xe nuclear spin destruction rate. This method was employed to determine the spin polarization $P_{^{129}Xe}$ at different temperatures, as presented in Table II. The disadvantage of this method lies in the difficulty to measure the Rb spin polarization accurately. However, our method directly measures the effective magnetic field produced by the ^{129}Xe nuclear spin polarization, thus becoming independent of the accuracy in measuring the Rb spin polarization. In comparison with measuring the initial induced voltage of the FID of the ^{129}Xe nuclei, the error is due to the variation of cell temperatures and conditions, the magnetic field gradient, the gas pressure and the pump and probe powers.

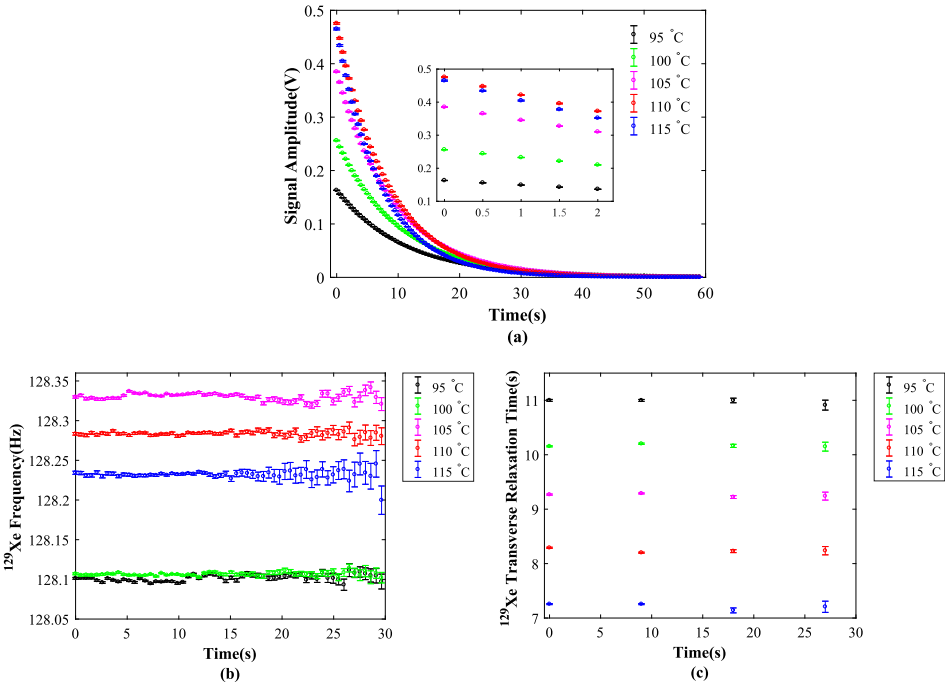

FIG. 5. (a) Fitting results of the FID voltage signal profile of ^{129}Xe at different temperatures using Eq.(12). The inset shows the magnification of FID profile at different temperatures in the time interval of 0–2 s. (b) The Larmor precession frequency drift of ^{129}Xe nuclei at different temperatures. (c) The transverse relaxation time drift of ^{129}Xe nuclei at different temperatures.

TABLE II. Magnetic field produced by ^{129}Xe at different temperatures.

			$P_{129_{Xe}}(\%)$	
T ($^{\circ}C$)	V_{FID} (V)	B_{FID} (nT)	our method	Refs. 16,17,27
95	0.163±0.00035	1.753±0.0039	0.612±0.0014	0.623±0.021
100	0.256±0.00059	2.535±0.0062	0.885±0.0022	0.897±0.029
105	0.385±0.0011	3.235±0.0096	1.129±0.0034	1.246±0.035
110	0.475±0.0015	3.545±0.011	1.238±0.0038	1.348±0.041
115	0.465±0.0018	3.059±0.012	1.068±0.0042	1.235±0.052

V. CONCLUSION

In this paper, we demonstrate a method for the direct determination of nuclear spin polarization by employing the effective magnetic field produced by the spin polarization of ^{129}Xe nuclei based on the atomic magnetometer. The effective magnetic field produced by the polarized of ^{129}Xe nuclei can be estimated by measuring the initial induced voltage of the FID signal. The advantage of this approach is that the method is not affected by inaccuracies in measuring of the Rb spin polarization, and the measurement only requires a few minutes. The measurement method demonstrated in this paper may facilitate the research on the temperature dependence of the ^{129}Xe nuclei, which can help us to improve the spin polarization of ^{129}Xe nuclei.

ACKNOWLEDGMENTS

This research was supported by the National High Technology Research and Development Program 863 (2014AA123401); by the National Natural Science Foundation of China (NSFC) (61673041 and 61227902); by the National Key R&D Program of China (2016YFB0501601); and by the Recruitment Program for Young Professionals (29816172).

[1] M. Rao, N. J. Stewart, G. Norquay, P. D. Griffiths, and J. M. Wild, Magn. Reson. Med. **75**, 2227–2234 (2016).
[2] G. Norquay, S. R. Parnell, X. Xu, J. Parra-Robles, and J. M. Wild, J. Appl. Phys. **113**, 044908 (2013).
[3] J. P. Mugler and T. A. Altes, J. of Magn. Reson. Imaging **37**, 313–331 (2013).
[4] C. Y. Jiang, X. Tong, D. R. Brown, S. Chi, A. D. Christianson, B. J. Kadron, J. L. Robertson, and B. L. Winn, Rev. Sci. Instrum. **85**, 075112 (2014).
[5] E. Karimi, L. Marrucci, V. Grillo, and E. Santamato, Phys. Rev. Lett. **108**, 044801 (2012).
[6] Z. D. Grujić, P. A. Koss, G. Bison, and A. Weis, Eur. Phys. J. D **69**, 135 (2015).
[7] R. Mhaskar, S. Knappe, and J. Kitching, Appl. Phys. Lett. **101**, 241105 (2012).
[8] K. Kamada, Y. Ito, S. Ichihara, N. Mizutani, and T. Kobayashi, Opt. Express **23**, 6976–6987 (2015).
[9] D. Meyer and M. Larsen, Gyroscopy and Navigation **5**, 75–82 (2014).
[10] Y. N. Pokotilovski, Phys. Lett. B **686** (2010).
[11] R. Sunier, T. Vancura, Y. Li, K. U. Kirstein, H. Baltes, and O. Brand, J. Microelectromech. Syst. **15**, 1098–1107 (2006).
[12] T. G. Walker and M. S. Larsen, Adv. At. Mol. Opt. Phys. **65**, 373–401 (2016).
[13] C. Cohen-Tannoudji, J. DuPont-Roc, S. Haroche, and F. Laloe, Phys. Rev. Lett. **22**, 758 (1969).
[14] V. V. Yashchuk, J. Granwehr, D. F. Kimball, S. M. Rochester, A. H. Trabesinger, J. H. Urban, D. Budker, and A. Pines, Phys. Rev. Lett. **93**, 160801 (2004).
[15] I. M. Savukov and M. V. Romalis, Phys. Rev. Lett. **94**, 123001 (2005).
[16] W. Shao, G. Wang, and E. W. Hughes, Phys. Rev. A **72**, 022713 (2005).
[17] G. Cates, R. Fitzgerald, A. Barton, P. Bogorad, M. Gatzke, N. Newbury, and B. Saam, Phys. Rev. A **45**, 4631 (1992).
[18] Z. Ma, E. Sorte, and B. Saam, Phys. Rev. A **106**, 193005 (2011).
[19] A. S. Barton, N. R. Newbury, G. D. Cates, B. Driehuys, H. Middleton, and B. Saam, Phys. Rev. A **49**, 2766 (1994).
[20] A. Korver, D. Thrasher, M. Bulatowicz, and T. G. Walker, Phys. Rev. Lett. **115**, 253001 (2015).
[21] S. Zou, H. Zhang, X. Y. Chen, and W. Quan, J. Korean Phys. Soc. **66**, 887–893 (2015).
[22] R. Slocum and B. Marton, IEEE Trans. Magn. **9**, 221–226 (1973).
[23] K. Kamada, Y. Ito, S. I. Chihara, N. Mizutani, and T. Kobayashi, Opt. Express **65**, 373–401 (2016).
[24] H. Y. Carr and E. M. Purcel, Phys. Rev. A **94**, 630 (1954).
[25] E. L. Hahn, Phys. Today **6**, 4–9 (1953).
[26] S. Schaefer, G. D. Cates, T.-R. Chien, D. Gonatas, W. Happer, and T. G. Walker, Phys. Rev. A **39**, 5613 (1989).
[27] X. Zeng, Z. Wu, T. Call, E. Miron, D. Schreiber, and W. Happer, Phys. Rev. A **31**, 260 (1985).